Glass-like phonon dynamics and thermal transport in a GeTe nanocomposite at low temperature

R. Cravero, A. Tlili, J. Paterson, M. Tomelleri, P. Marcello, R. Debord, S. Pailhès, O. Bourgeois, F. Hippert, D. Le Qui, et al.

Glass-like phonon dynamics and thermal transport in a GeTe nanocomposite

R. Cravero,[1,2] A. Tlili,[1] J. Paterson,[3] M. Tomelleri,[3,1] P. Marcello,[1] O. Bourgeois,[2] F. Hippert,[4] D. Le Qui,[5] J.-Y. Raty,[5] P. Noe,[3] and V. M. Giordano[1]

[1] *Institute of Light and Matter, UMR5306 Université Lyon 1-CNRS, Université de Lyon, F-69622 Villeurbanne cedex, France*
[2] *Institut NEEL, CNRS, Université Grenoble Alpes, 25 avenue des Martyrs, F-38042 Grenoble*
[3] *Université Grenoble Alpes, CEA, LETI, 38000, Grenoble, France*
[4] *Université Grenoble Alpes, CNRS, Grenoble INP, LMGP, Grenoble F-38000, France*
[5] *FNRS and CESAM, Université de Liége, 4000 Sart-Tilman, Belgique*

With advances in nanoelectronics, and the need of novel and more efficient energy harvesting solutions, thermal management has arisen as one of the most urgent challenges. To reduce heat dissipation and improve the thermoelectric efficiency, the ultimate goal is a material with a glass-like thermal conductivity but still good electronic properties. Nanostructuration is one of the most promising strategies to get such material, as nanoscale interfaces are expected to strongly scatter the lattic vibrations with comparable wavelength with a lesser effect on electrons. Recent simulations have reported a glass-like phonon dynamics and thermal transport in amorphous/crystalline composites, suggesting a parallelism between glasses and nanocomposites, due to the presence in both of elastic heterogeneities. Here we report the experimental evidence of a glassy phonon dynamics, specifically the arising of an excess intensity in the low energy phonon density of states, together with a glass-like lattice thermal conductivity in a GeTe-based nanocomposite of interest for microelectronics. We show that these features are the consequence of the presence of elastic heterogeneities due to the nanostructuration and a dominant interface scattering leading to a diffusive thermal transport. Our findings open new perspectives in phonon and thermal engineering through the direct manipulation of elastic heterogeneities.

I. INTRODUCTION

Nanostructured materials are at the forefront of current research for many applications, specifically, those where thermal management represents an issue, such as thermoelectric energy conversion or microelectronics. Here the challenge is to reduce the thermal conductivity without affecting the electronic properties. For this, the aim is to reduce the heat transport assured by the lattice vibrations, whose quasi-particle is the phonon, while perturbing as least as possible the electronic contribution. In one word, it is matter of finding the "phonon glass electron crystal" ideal material [1], *i. e.* a material which is as bad a thermal conductor as a glass but still a good electric conductor as a crystal. The introduction of interfaces at the nanoscale (from few to hundreds of nm) represents a most promising strategy as they are expected to efficiently scatter phonons, with a lesser effect on electrons. Still, things are not this clear when it comes to nanocomposites, made of the intertwining at the nanoscale of materials with different properties, where not only interfaces are present, but also nanoscale heterogeneities in elastic and thermal properties. Such combination can lead to very different thermal behaviors, from the enhancement of the thermal conductivity [2–5] to its strong inhibition [6–13], depending on the constituent materials properties, as well as the nanostructure length-scale and the temperature[14]. Simulations have shown that this panoply of behaviors is due to the non trivial effects of nanoscale heterogeneities on phonons [15–18], which can also lead to phonon localization [19] or filtering [20]. Most interestingly, the arising of glass-specific features in the vibrational dynamics has been observed in molecular dynamics simulations on nanocomposites made of nanocrystalline inclusions within an amorphous matrix. Specifically, it was reported an early deviation of the low frequency phonon density of states from the Debye behavior, leading to a peak reminiscent of the Boson Peak in glasses, well distinct from the Boson Peak of the amorphous matrix [16]. Similarly to this latter, this deviation appears together with a change of the nature of the phonon from propagative to diffusive. As such, simulations point to these nanocomposites as a possible realization of the phonon glass electron crystal. Moreover, while the nature of the Boson Peak in glasses is still matter of debate, one of the proposed interpretations ascribes it to a strong phonon scattering due to the presence of nanometric elastic heterogeneities intrinsic to the disordered state [21–23]. This would suggest a parallel between glasses and nanocomposites, due to the presence in both of elastic heterogeneities, intrinsic to the disorder state in the former and artificially induced in the latter. Such concept, if confirmed, could open new exciting perspectives in phonon thermal engineering. Unfortunately, until now, an experimental confirmation is still missing.

Here we produce the first experimental evidence of the arising of glass-like dynamics and thermal transport due to nanoscale elastic heterogeneities in a nanocomposite based on germanium telluride (GeTe), of interest for microelectronic, photonic and thermoelectric applications.

GeTe belongs to the family of chalcogenide materials at the forefront of current research for phase change resistive memories (PCM) in microelectronic devices [24–26], neuromorphic computing [27], laser thermal lithography [28], optically photonic devices [29] as well as for thermoelectric applications [30–32]. This family has

been reported to exhibit a novel kind of atomic bonding, dubbed metavalent, considered to be responsible for a series of properties which make it especially interesting for PCMs and thermoelectrics [33]. In both these applications, the major challenge for reducing energy consumption in the former and improving the figure of merit in the latter, is the reduction of the thermal conductivity. The main strategy has been to increase phonon scattering by doping or alloying [32, 34]. In some cases the deposited amorphous alloy has led, upon crystallization, to a phase segregation and the realization of nanodomains of the undoped phase change material separated by another phase. It's the case of $Ge_2Sb_2Te_5$-SiO_x nanocomposites, for which a twofold thermal conductivity reduction was reported for a 5% SiO_x molar content [35]. Very recently, the crystallization of carbon doped GeTe has also been shown to give rise to a nanocomposite made of nanograins of crystalline GeTe (below 20 nm size) interconnected by amorphous carbon, which has proved to efficiently reduce the programming currents in PCM devices, suggesting an important thermal conductivity reduction [36–38]. This, together with an increased thermal stability, due to a higher crystallization temperature in the nanocomposite, points to this material as very promising for PCM applications. Still, to optimize its composition and nanostructure, a microscopic understanding of the effect of this latter on thermal transport is necessary.

Disentangling the many elements which play a role in determining heat transport in GeTe is however not trivial. In bulk GeTe thermal transport is dominated by anharmonic phonon-phonon scattering and scattering from Ge vacancies [39, 40], which are naturally created during crystallization from the amorphous phase, making of GeTe a p-type semiconductor [41]. These mechanisms will be present in the nanocomposite as well, and possibly different. As such, upon nanostructuration, four are the main players: i) Ge vacancy content, ii) anharmonicity, iii) grain size and iv) the nanoscale heterogeneities due to the contrast of properties between GeTe and amorphous carbon.

In this work we adress these nanocomposites in order to shed light on the microscopic mechanisms behind thermal transport and evidence the effect of the nanostructure. We find that nanostructuration leads to a lattice thermal conductivity between 4 and 7 times smaller than in pure GeTe, for 9% atomic carbon content. Such reduction cannot be explained on the basis of the nanometric grain size or of defect scattering alone, pointing to a major role of boundary scattering whose strength is enhanced by the elastic contrast between the components. Such enhanced scattering leads to the appearance of an excess of modes in the vibrational density of states at wavelengths comparable with the nanostructure length-scale and to a glass-like lattice thermal conductivity, that we interpret as the result of a dominant diffusive thermal transport.

II. RESULTS

A. Samples

Here we present a thorough investigation of thermal transport and phonon dynamics in a C-doped GeTe thin film with a 9% carbon atomic content (GTC9), compared with the ones in a pure GeTe thin film (GeTe). In order to verify the role of grain size and carbon content we have also prepared a nano-crystalline GeTe (nGeTe) and a nanocomposite with a 16% carbon atomic content (GTC16) for specific measurements. As detailed in Methods, all samples have been deposited as homogeneous amorphous materials and then crystallized through a controlled annealing up to 500 °C for the nanocomposites and 450 °C for GeTe. In all samples, crystallization of GeTe is accompanied by the expulsion of the excess Ge, which crystallizes at slightly higher temperature (see Methods). Upon crystallization C-doped GeTe expells also carbon, leading to the formation of a nanocomposite made of nanometric crystalline grains of GeTe surrounded by amorphous carbon [38]. nGeTe was prepared by interrupting the annealing just after the crystallization of the expelled Ge, as monitored by reflectivity measurements, and by quenching the sample to avoid any further grain growth. All samples were investigated by x ray diffraction (reported in Supplementary Material), allowing us to confirm the rhombohedral structure of the GeTe phase in all of them. The grain size, as obtained using the Scherrer law, is reported in Table I, together with the mass density, measured by x ray reflectivity. The crystalline peaks of expelled Ge are also always present, from which we can estimate an average Ge grain size d_{Ge} = 50.5(9) nm in GeTe and d_{Ge} =23(7), 15(4) and 18(10) nm in nGeTe, GTC9 and GTC16 respectively.

Concerning the amorphous carbon (a-C) present in the nanocomposites, it is important to estimate its density and fraction of sp^3 bonded carbon atoms, as density, sound velocity and thermal conductivity strongly depend on these quantities [42–44]. In order to estimate the sp^3 fraction in GTC9, we have measured its Raman spectrum in the frequency region of the amorphous carbon stretching modes. The sp^3 fraction can be estimated from the intensity ratio between the two Raman peaks (see Supplementary Material) [45], and the width of the G peak is related to carbon density. We find that our spectrum is compatible with a mostly sp^2 bonded material (60%), and a density of about 2 g·cm^{-3}. We can now calculate the carbon volume fraction starting from the atomic concentration and the amorphous carbon density. In the literature this latter spans from 1 to 3 g·cm^{-3} [42], leading to a volume fraction ψ_{a-C} between 2 and 7% for GTC9 and between 4 and 12% for GTC16. For our estimated carbon density, ρ = 2 g·cm^{-3}, it is ψ_{a-C}=3% for GTC9 and ψ_{a-C}=6% for GTC16. Based on the elasticity data reported in the literature for our estimated density [46], the average Debye velocity for amorphous carbon is ∼8.6±1.5 Km/s. Knowing the Debye velocity for

	GeTe	GTC9	GTC16	nGeTe
grain size (nm)	80(10)	16(3)	13(3)	30(5)
density (g/cm^3)	6.24(4)	5.86(4)	5.73 (4)	5.76(3)
ρ ($\mu\Omega$ cm)	580(1)	1390(1)		
$n_H(10^{20}cm^{-3})$	2.7(1)	11.1(1)	11.5(1)	
k_T (W/m·K)	3.8(1)	1.39(7)		3.1(8)
k_{el} (W/m·K)	1.310(3)	0.5251(5)		
k_{ph} (W/m·K)	2.5(6)	0.86(7)		

TABLE I. Structural, electrical and thermal properties for the samples here investigated. The thermal conductivity was measured by the 3ω technique in all samples, except for nGeTe, for which we used the thermoreflectance technique (see Methods).

GeTe, $v_{GeTe} \sim 1.9$ Km/s [47], we can calculate the elastic contrast between the two phases, as the ratio between their acoustic impedences $Z = \rho^M v$, $\chi = \frac{Z_{a-C}}{Z_{GeTe}} \sim 1.5(2)$. We are thus in presence of a good elastic contrast, with the crystalline particles softer than the amorphous network.

B. Thermal conductivity

Fig. 1 (a) reports the thermal conductivity of GeTe, GTC9 and amorphous GeTe as a reference for the lowest possible thermal conductivity in pure GeTe. First of all, we remark the very good agreement between our data on GeTe and previous measurements on both amorphous and crystalline GeTe thin films, also reported in the figure [40, 48]. The differences can be ascribed to a variable content of Ge vacancies, as a consequence of a different Ge/Te ratio in the as deposited state resulting from sputtering target composition and deposition method. The weaker than 1/T temperature dependence was already reported and ascribed to the combination of Umklapp anharmonic phonon-phonon scattering and vacancy scattering [39, 40].

Concerning GTC9, we observe a strong reduction of the thermal conductivity with respect to GeTe, by a factor of 7 at low temperature and 4 at room temperature and an opposite temperature dependence: rather than decreasing, it slightly increases with temperature. In order to extract the lattice contribution to thermal conductivity, we have measured the electrical conductivity σ and calculated the electronic contribution as : $k_{el} = L\sigma T$, with T the temperature and L the Lorenz number (Wiedemann-Franz law) [49]. As a first approximation, we have extrapolated to our temperature range the Lorenz number calculated in Ghosh *et al.* for GeTe in the [322-503] K temperature range [40], reported in the Supplementary Material. Parallely, we have also calculated it using $L = (1.5 + e^{-|S|/116}) \cdot 10^{-8}$ WΩ/K^2 [50] and our measured Seebeck coefficient S [51], and found that both methods lead to the same result within error bar.

The electronic contribution, reported in Fig. 1 (b), decreases by a factor between 2.5 and 3.5 going from GeTe to GTC9. This is due to a drastic mobility reduction, as the carrier concentration n_H measured by Hall effect and reported in Table I is found to increase by almost a factor of 4 in GTC9. As holes are provided by Ge vacancies, this increase is due to a larger vacancy content in nanocomposites, likely due to a "Ge-drag" effect during the slow segregation of carbon atoms upon GeTe crystallization. The increased defect scattering from vacancies for holes would thus contribute to reduce the mobility.

Looking now to the pure phononic contribution, reported in Fig. 1 (c), we find that, going from GeTe to GTC9, it decreases by a factor as large as 6 at low temperature and 3 at room temperature. Most surprisingly, the GTC9 lattice contribution is found to increase with temperature, with a similar dependence as in amorphous GeTe, suggesting a glass-like thermal transport in this nanocomposite.

C. THz phonon dynamics

In the Boltzmann transport theory within the single relaxation time approximation, the vibrational contribution from propagative modes to thermal conductivity can be expressed as an integral over all phonon frequencies [52, 53]:

$$k_{ph}^{prop} = 1/3 \int C_v(\omega) v^2(\omega) \tau(\omega) g(\omega) d\omega; \qquad (1)$$

with $C_v(\omega)$ and $g(\omega)$ the phonon specific heat and density of states, v its group velocity and τ its lifetime, measuring the average time between two inelastic scattering processes.

In order to get a better insight on the microscopic mechanisms leading to the strong modification of thermal transport when going from GeTe to GTC9, we have directly looked at individual phonons, by measuring the high frequency vibrational dynamics by Inelastic X-ray Scattering (IXS) at the ID28 beamline of ESRF. Measurements were performed at room temperature on GeTe, GTC9 and also GTC16 to see the effect of a major carbon content. We report in Fig. 2 some representative spectra of the individual phonons for GeTe and GTC9, as collected by IXS at fixed wavevectors q. As our samples are polycrystalline, phonons are measured in the first Brillouin zone and correspond to the orientational average of the branches over all directions [54].
The intensity of GTC9 data has been rescaled to be exactly on the top of the GeTe ones. In all spectra we can identify a well defined peak, with a high energy shoulder appearing at larger wavevectors: going from GeTe to GTC9 introduces only minor changes and mostly localized on the high energy shoulder. Increasing the C content from 10 to 16% does not introduce any relevant difference (reported in the Supplementary Material).

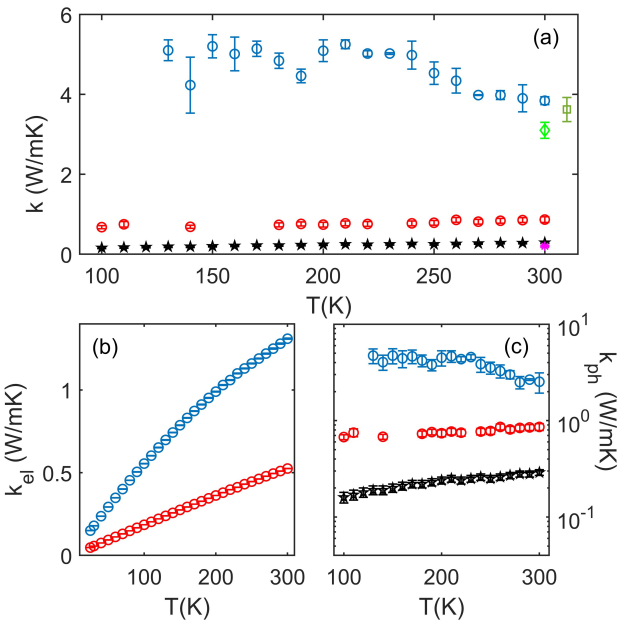

FIG. 1. **Thermal conductivity**. (a) The thermal conductivity as measured by the 3ω technique is reported for GeTe (blue circles), GTC9 (red circles squares) and amorphous GeTe (black stars). Literature data for crystalline GeTe (dark green square [40], light green diamond [48]) and amorphous GeTe (magenta asterisk [48]) are also reported for comparison. Error bars are obtained taking into account the experimental uncertainties on all parameters of the model, using a Monte Carlo procedure, as explained in the Supplementary Material. (b) The electronic contribution to thermal conductivity, calculated from the measured electrical conductivity, is reported for GeTe and GTC9. (c) The lattice contribution is reported for GeTe, GTC9 and amorphous GeTe in a logarithmic scale to enhance the visibility of the temperature dependences. Error bars are obtained by error propagation on the total thermal conductivity and the electronic contribution.

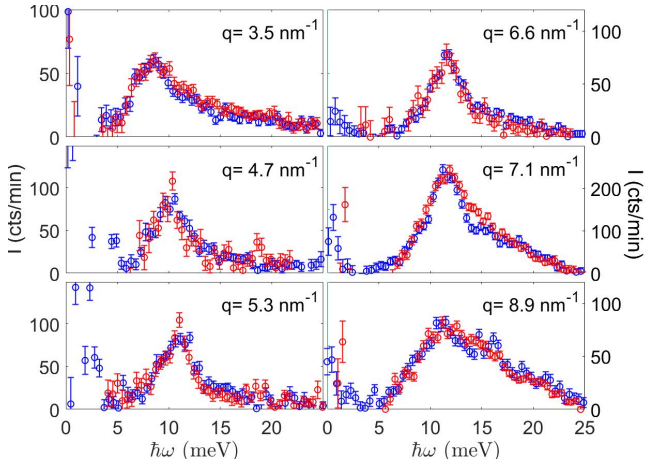

FIG. 2. **Inelastic scattering spectra**. Some representative inelastic scattering spectra collected on GeTe (blue circles) and GTC9 (red circles) are reported at the wavevector values indicated in each panel. GTC9 spectra have been rescaled on the GeTe one to easy the comparison. For better visibility, spectra have been subtracted of the elastic line, and we only show the positive exchanged energy side. Error bars correspond to the Poissonian error on the scattered intensity.

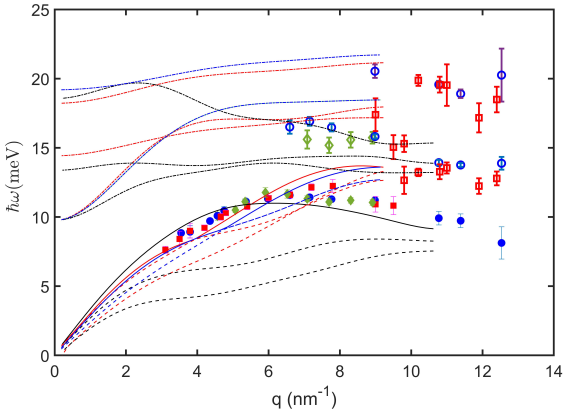

FIG. 3. **Phonon dispersions** The experimental phonon energy $\hbar\omega$ with respect to wavevector in absolute units q are reported for GeTe (blue bullets), GTC9 (green bullets) and GTC16 (red bullets), together with *ab initio* calculations for the main symmetry directions in pure GeTe at 0 K (dashed lines: transverse acoustic phonons, solid lines: longitudinal acoustic: phonons, dot-dashed lines: optic modes): $\Gamma - L$ (red), $\Gamma - X$ (black), $\Gamma - T$ (blue) (see Methods for their definition). Experimental data correspond to the average of different longitudinal branches over all directions.

We have fitted these data using a model with a variable number of excitations, from 1 to 3 depending on the q value, all represented by a Damped Harmonic Oscillator (DHO) (see Supplementary Material). Our results for the phonon dispersions are reported in Fig. 3 together with the theoretical ones calculated *ab initio* for a pure GeTe at 300 K. It is worth noticing that our data represent the first experimentally measured phonon dispersions in rhombohedral GeTe. It may be seen that GeTe data are in a very nice agreement with calculations: the low energy mode can be identified as a longitudinal acoustic mode, averaged over the longitudinal branches. The high energy shoulder is made of several modes belonging to different optic branches. In our experimental geometry we are mostly sensitive to longitudinal density-density fluctuations. Still, in polycrystalline materials, towards the end of the Brillouin zone, it is usually possible to see also transverse modes. It is not our case. The lower energy ones are likely hidden by the intense elastic line, while the higher energy ones could be indistinguishable from the longitudinal ones within their experimental width [54]. Overall, GTC9 and GTC16 well overlap the GeTe data, with no significant differences in the energy position, nor in phonon broadening, as can be seen from Fig. 2. It is worth reminding here that in polycrystalline samples the observed phonon linewidth is made of three contributions: the experimental resolu-

tion, the width of the phonon distribution over all directions, i.e. the inter-branches separation, and finally the intrinsic phonon broadening, inversely proportional to phonon lifetime [53, 54]. In our case, the experimental broadening in the acoustic region is fully determined by the former two contributions, *i.e.* we could not extract a phonon intrinsic linewidth. Our experimental conditions set in fact a low limit for the detectable intrinsic width which lies between 0.6 and 1.5 meV depending on q, corresponding thus to an upper limit on the detectable phonon lifetime and mean free path of 1 - 2 ps and $\sim 5-10$ nm respectively [53]. The real intrinsic width and mean free path are therefore respectively below and above such limits, so that we can only conclude that phonon mean free path in both GeTe and GTC9 is longer than 5-10 nm.

Despite the sizable effect on thermal transport, which clearly points to a major change in phonon dynamics, we do not observe it within our experimental resolution. However, such change is expected to mostly concern phonons with wavelengths comparable to the nanostructure lenghscales: the amorphous carbon thickness and the GeTe grain size, *i.e.* between 1 and $\sim$ 16 nm [38]. These wavelengths could not be accessed in our experiment because of the strong small angle scattering, the smallest measured wavevector being $q = 3.5$ nm^{-1}, corresponding to a maximum phonon wavelength $\lambda = 1.8$ nm. In order to access this scale, corresponding to energies smaller than 7 meV, we have measured the vibrational density of states (DOS) using the Inelastic X-ray Scattering technique with Nuclear resonance Analysis (IXS-NRA) at the ID18 beamline of ESRF [55]. Measurements have been performed at 50 K, for avoiding any spurious effect coming from the multi-phonon contribution subtraction at temperatures higher than the Debye temperature, which is around 180 K for GeTe [39]. Some room temperature scans have also been collected on GeTe and GTC16 for following the modification of the DOS with temperature (shown in the Supplemenary Material). Previous data in the literature have been reported only on the partial Te density of states at 30 K, using the same technique [47], and on the neutron-weigthed density of states of a powder GeTe bulk sample at room and higher temperature [56]. A comparison is reported in the Supplementary Material, showing a reasonable agreement. In Fig. 4 we report the DOS as measured in GeTe, compared to the theoretically calculated one (panel (a)) and to GTC9 and GTC16 (panel (b)), all of them measured at 50 K. Once again we notice the very good agreement with our theoretical results for pure GeTe. Referring to Fig. 3, we can easily identify the dip at ≈ 13 meV as the end of the acoustic regime, the large maximum preceding it corresponding to the different Van Hove singularities coming from longitudinal and transverse branches in the various directions. The two other bands, centered at 16 meV and 20 meV correspond to bundles of optic modes, that we have measured by IXS.

The DOS is significantly modified in the nanocomposites. It is worth mentioning that, for GeTe, the integrated DOS up to 32 meV is here normalized to 1, as all modes lie in the investigated energy range. This is not true for GTC: additional modes are present at larger energies, due to the amorphous carbon component. Still, the carbon modes give only a negligible contribution below 30 meV, so that the total area of our measured DOS below 32 meV is basically proportional to the GeTe concentration in GTC: 0.91 for GTC9 and 0.84 for GTC16, as we confirmed with theoretical calculations. We have thus accordingly normalized the integrated DOS for the nanocomposites reported in Fig. 4. Besides the different area, the evident difference in the DOS of the nanocomposites is an overall broadening, as well as a slight downshift of the optical bands with respect to GeTe. In order to better inspect the acoustic region, we report in panel (c) the DOS normalized to the expected Debye dependence at low energy: $g(\hbar\omega)/(\hbar\omega)^2$. While in GeTe we observe the expected Debye behavior up to $\sim 4-5$ meV, this is not the same in the nanocomposites: low energy intensity starts to raise already at our lowest measured energy point (2 meV for GTC9 and 1.6 meV for GTC16), leading to an excess of intensity over the Debye level at about 4 meV before reaching the acoustic Van Hove singularity. Moreover, this excess intensity, reminiscent of the Boson peak in glasses, increases with carbon content.

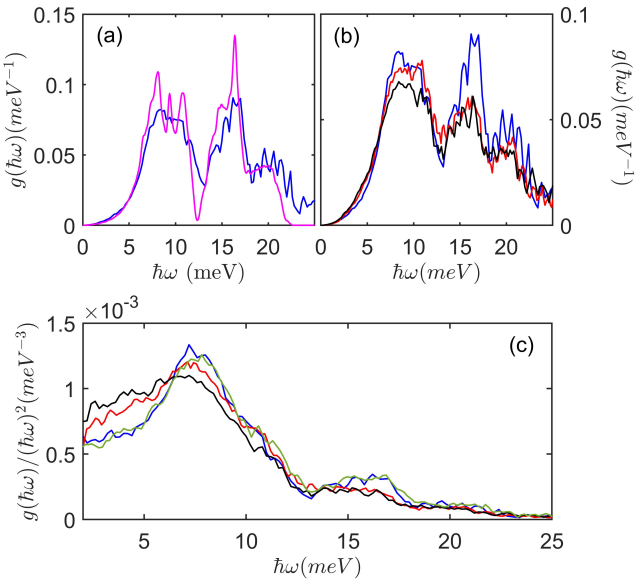

FIG. 4. **Phonon density of states** (a) Phonon density of states as measured using the IXS-NRA technique on GeTe at 50 K (blue) compared with the one calculated *ab initio* (magenta). (b) Phonon density of states at 50 K for GeTe (blue), GTC9 (red) and GTC16 (black). A general broadening is observed in the nanocomposite, as well as modifications in the acoustic regions. (c) Reduced phonon density of states for GeTe (blue), nGeTe (green), GTC9 (red) and GTC16 (black), showing the growing up of an excess intensity in the 5 meV region in the nanocomposite, increasing with carbon content.

This perturbed energy range corresponds to the perturbation of acoustic phonons with wavelengths between 2.5 and 10 nm, *i.e.* within the range expected to be affected by nanostructuration.

III. DISCUSSION

We have seen that the nanocomposites exhibit both glassy phonon dynamics and glassy thermal conductivity behavior. Going from GeTe to GTC, there are several structural modifications which add to phonon scattering: 1) grain size is reduced from 80 to $\sim$ 15 nm; 2) the vacancy content increases by a factor of 4; 3) there are heterogeneities of elastic properties at the nanoscale because of the presence of amorphous carbon. In order to disentangle the effect of all these modifications on dynamics and thermal transport, we have first investigated a nanocrystalline GeTe sample (nGeTe), with average grain size 30(5) nm. On one hand, the room temperature thermal conductivity is indistinguishable within error bars from the one of GeTe, as reported in Table I. On the other hand, the phonon density of states, also reported in Fig. 4 (c), still follows at low energy the Debye behavior. It could be possible that modifications in the DOS could arise only for a smaller grain size, such as in the nanocomposites ($\sim$ 15 nm). Still, the excess intensity at low energy increases with carbon content, although grain size is almost unchanged between GTC9 and GTC16, suggesting thus that this parameter is not responsible for the observed modifications. The same considerations hold for the role of vacancy scattering or scattering from expelled Ge nanograins, as the vacancy content and Ge grain size remain almost constant with carbon content in the nanocomposites. We can thus conclude that the excess of modes in the low energy vibrational density of states and the drastic change in the thermal conductivity behavior are the consequence of the presence of amorphous carbon.

In order to estimate the relative importance of the carbon effect over grain size and vacancy scattering, we fit our thermal conductivity data using Eq. 1 limited to acoustic modes and our experimental results for phonon dispersions and density of states. Phonon lifetime can be calculated using the Mathiessen rule, $\frac{1}{\tau} = \Sigma_i \frac{1}{\tau_i}$, where τ_i is the lifetime associated to the i scattering process. We consider 3 contributions (anharmonic Umklapp scattering, defect scattering from vacancies and scattering from grain boundaries):

$$\tau_U(\omega,T)^{-1} = B\omega^2 T e^{-\frac{\Theta_D}{3T}}$$
$$\tau_{def}(\omega)^{-1} = \frac{\Gamma_{\rm def}(\omega)}{2\hbar}$$
$$\tau_{GB}^{gray}(\omega)^{-1} = \frac{1}{P_{GB}}\frac{v_g(\omega)}{d}$$

where B is the strength of Umklapp scattering and Θ_D=180 K [39] is the Debye temperature in GeTe. In order to model the lifetime contribution due to defect scattering, we need to model the defect induced attenuation Γ_{def}, for which we use a simple analytical model successfully used in mass disorder alloys [57, 58]: this gives $\Gamma_{\rm def} = \pi/2(\hbar\omega)^2 g(\hbar\omega)\langle\epsilon^2\rangle$, where $g(\hbar\omega)$ is the DOS, and ϵ represents the sum of all fluctuations contributions (mass, elastic constants, atomic size) [59]. Using this model, we find that the expected phonon broadening due to Ge vacancies does increase going from GeTe to the nanocomposites, as expected. However, it remains below 0.15 meV, corresponding to lifetimes much longer than 10 ps, which is the reason for which we could not observe it in our IXS experiment. Concerning scattering from grain boundaries, the phonon mean free path will be proportional to the average grain size d (and thus phonon lifetime proportional to d/v_g with v_g the group velocity), weigthed by a factor P_{GB} which takes into account the transmission through the grain boundaries as well as the quality of the interface. As a first approximation we have used the largely used 'gray' model, where the parameter P_{GB} accounts for the effect of grain boundary transmission, though neglecting its energy dependence, which has been found to be relevant mostly at temperatures lower than ours [60]. We note that in this calculation we have only used the average longitudinal acoustic dispersion measured, which however is quite representative of an average acoustic dispersion, as theoretical calculations show that many transverse branches have energies similar to the longitudinal ones. As we show in the Supplementary Material, using longitudinal and transverse branches calculated by DFT changes only slightly the values of the fitted parameters, without modifying the physical result. For the density of states, we have used the experimental one measured at 50 K. We have checked that using the one at 300 K there is no much difference. Indeed the acoustic region is almost unchanged upon temperature, as shown in the Supplementary Material.

As can be seen in Fig. 5, this model gives a good match of the experimental data for GeTe, with $B = 6.6(8)\cdot 10^{-5}$ (meV·K)$^{-1}$, and P_{GB}=0.30(8). A reduced transmission, as indicated by the value of P_{GB}, accounts here for the interface roughness, the crystalline orientation mismatch between neighboring grains and the presence of porosity.

As a first step, we neglect the nanocomposite nature of GTC9, and estimate the effect of a reduced grain size and increased vacancy content on thermal conductivity, using the parameters B and P_{GB} identified for GeTe, and grain size and density of states of GTC9. This estimation is reported in Fig. 5 (b) as a black dashed line: it clearly lies well above the experimental one, and keeps a decreasing temperature dependence, confirming that these two scattering sources are not sufficient for inducing the observed thermal transport modification.

As a second step, we consider GTC9 as a GeTe material with "thick and decorated" grain boundaries, including the effect of the amorphous component in an en-

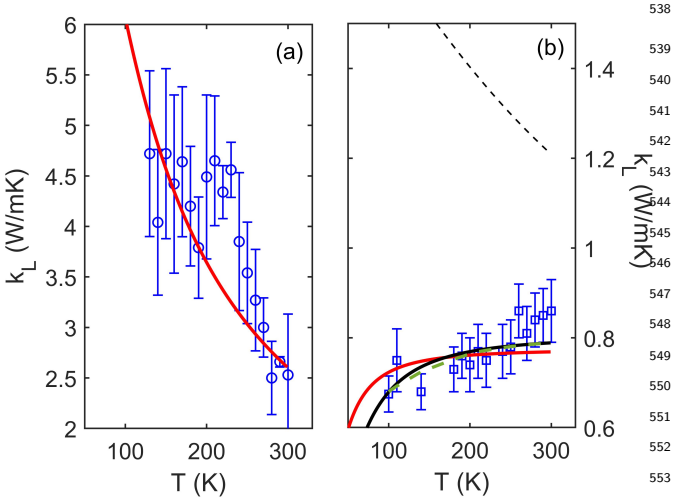

FIG. 5. Fit of experimental thermal conductivity. (a) The lattice thermal conductivity of GeTe is reported together with the fit Eq. 1 and the gray model for boundary scattering (red solid line). (b) the lattice thermal conductivity of GTC9 is reported together with the estimated thermal conductivity from GeTe just changing defect scattering and grain size (dashed-dotted black line). The thick red solid line is the fit with Eq. 1 and the gray model for boundary scattering, letting the Umklapp parameter go to 0. The thick black solid line is the same fitting with the addition of a diffusive optic contribution. The thick green dashed line represents the fit with an EMA approach, including the Kapitza interfacial resistance.

hanced boundary scattering. For this, we let free both the phonon transmission, which will now be related to the elastic contrast between GeTe and amorphous carbon, and the anharmonic scattering parameter. Indeed, the slight softening of the optic bands in the nanocomposite DOS suggests a possibly higher anharmonicity. As can be seen in the figure, the fit with this model is not able to reproduce the temperature dependence of the experimental data, despite it decreases the Umklapp parameter down to zero. As for the grain boundary scattering, it results P_{GB}=0.084(4), *i. e.* a ∼70% reduction of the transmission at boundaries: this is the expected stronger boundary scattering due to the elastic contrast at the interfaces. It is worth noticing that the same value for P_{GB} is obtained even if we impose a positive value for B. While this lower transmission may help understanding the absolute value of the thermal conductivity, it cannot explain its temperature dependence. This latter clearly points to a thermal transport dominated by diffusive contributions, that we have not modelled here, where we have only used the propagative acoustic dispersions. Using the theoretical dispersions, we have estimated the diffusive contribution coming from the optical branches and found that it represents less than 10% of the total thermal conductivity in GeTe, but up to 27% in GTC9 at room temperature. We have thus performed the same fit but including the diffusive contribution from optical modes in GTC9, thus fitting our data with $k_{ph} = k_{ph}^{prop} + k_{ph}^{diff}$, where k_{ph}^{diff} is the diffusive contribution from optic modes described in the Supplementary Material. In this way, we obtain the black solid line reported in the figure, with $P_{GB} = 0.054(3)$ and B once again equal to 0. The agreement with experimental data is much better, especially at the lowest temperatures and an increasing behavior is now more pronounced. Still, this model neither cannot fully account for the experimentally observed increase. The residual diffusive contribution comes likely from a nanocomposite effect.

A dominant diffusive thermal transport and a thermal conductivity increasing with temperature was indeed reported in amorphous/crystalline silicon nanocomposites, although for much larger amorphous contents, of 50 and 70% [16, 61, 62]. The temperature increase was ascribed to the predominance of diffusive vibrational modes and to the Kapitza interface resistance, which decreases with temperature.

We have tried then an effective medium approach (EMA) by fitting our GTC9 data starting from the thermal conductivities of GeTe, modified for the grain size and vacancy content as in Fig. 5 (b), and the thermal conductivity of an amorphous carbon with similar density and sp^3 content as ours from litterature [42]. In order to account for the Kapitza interface resistance, R_K, we have used the formulation by Minnich *et al.* [63], with the thermal boundary resistance as only free fitting parameter. As reported in the Supplementary Material, the best fit is obtained assuming a linear dependence of the interfacial thermal conductance on temperature, *i.e.* $R_K = \frac{1}{A+BT}$, with A=100(10) MW·K^{-1}m^{-2} and B=0.44(6) MW·K^{-2}m^{-2}. The order of magnitude for the obtained interfacial thermal conductance is compatible with typical values for a mild contrast of properties [64]. The fit is reported in Fig. 5, showing an agreement similar to the one obtained including optic diffusive modes. It is worth noticing that in this EMA approach we could not account for a larger weigth of the optic diffusive contribution, which could be at the origin of the remaining discrepancies.

Our data could thus be explained on the basis of a mainly diffusive thermal transport mechanism. On one side, the propagative contribution is reduced due to scattering from defects and interfaces, thus giving a major weigth to the diffusive contribution from optic modes. On the other side, these latter cannot account for the whole diffusive contribution, which is related to a dominant interface scattering, which can be modelled with the Kapitza resistance. From a microscopic point of view, it likely leads to a change of nature from propagative to diffusive of the GeTe modes with energies corresponding to the excess intensity in the DOS, in agreement with the theoretical predictions [16]. In our case, however, phonons with higher energy are still propagative, as we have seen in our IXS measurements, suggesting an effect of the nanostructure limited to phonons with wavelengths longer than 2 nm (and energies corresponding to the DOS

excess intensity), which are mostly diffusively scattered at the interfaces. Molecular dynamics simulations on the real system are planned for identifying the effect of the nanostructuration on such phonons and the origin of the diffusive thermal transport.

IV. CONCLUSIONS

We have presented an experimental study of thermal transport in a GeTe nanocomposite made of nanograins of crystalline GeTe intertwinned with amorphous carbon, combining the macroscopic measurement of thermal conductivity with the microscopic investigation of phonon dynamics in the meV energy range. We have found that, the total thermal conductivity is reduced by a factor of 7 at low temperature and 4 at room temperature, due to a concomitant reduction of both electronic and lattice contributions. This latter, of only 0.87(7) W/mK at room temperature, exhibits a glass-like behavior, increasing with temperature. We have shown that, the low value of the lattice thermal conductivity can be explained by an enhanced boundary scattering, whose strength is much larger than in nanocrystalline GeTe, due to the elastic contrast with amorphous carbon. The glass-like temperature dependence can be understood in terms of a dominant role of boundary scattering and diffusive vibrational modes, as already reported in theoretical studies on amorphous/crystalline nanocomposites [16, 61, 62]. Indeed, not only the diffusive contribution from optic modes becomes more important in GTC9 with respect to GeTe, but also, similarly to the molecular dynamics studies, an excess intensity is found in the density of states at wavelengths comparable with the nanostructure lengthscale, suggesting that acoustic modes with those energies are strongly scattered by the elastic nanoheterogeneities and loose their propagative character contributing thus diffusively to thermal transport. It is worth underlying that in this nanocomposite the amorphous limit has not been achieved yet: the lattice contribution in GTC9 remains 3 times larger than the one in amorphous GeTe. As the DOS excess intensity becomes more important with increasing carbon content, an even more diffusive behavior could be expected in richer carbon nanocomposites, which could thus allow to achieve the amorphous limit.

These results give an experimental evidence of a glass-like phonon dynamics and thermal transport in a nanocomposite, which confirms the many recent theoretical results and allows to assess the parallelism between nanocomposite and glasses, due to the presence in both of elastic heterogeneities. As such, our findings open the way to the possibility of engineering materials with glassy thermal features by directly manipulating the distribution of the elastic heterogeneities: tuning its strength by choosing the component materials, thus the elastic contrast, and selecting the wavelength range of the affected phonons by choosing the nanostructure lengthscale.

V. METHODS

A. Sample synthesis and characterization

Thin films of variable thickness of the homogeneous amorphous alloy $GeTe_{1-x}C_x$ (GTC) have been synthesized by magnetron co-sputtering from a GeTe and a C target in Argon atmopshere on a 200 nm silicon wafer. For electric measurements, a 500 nmm SiO_2 layer was added on top of the wafer. All the films were then capped *in situ* with 20 nm amorphous SiN for avoiding any oxidation. Two C atomic contents were studied in this work, 9.1 (GTC9) and 16% (GTC16), and obtained by changing the relative sputtering powers applied to the two targets. The Ge and Te concentrations were assessed by Rutherford Back Scattering (RBS), while the one of C by Nuclear Reaction Analysis (NRA). The thickness and density were measured by X-Ray Reflectivity both at the CEA-LETI and at SOLEIL synchrotron radiation source, at the DiffABS beamline (XRR). A thermal annealing with a ramp rate of 10K/min was performed for inducing crystallization, while monitoring *in situ* the electrical resistivity by a 4 point probe method. The dramatic decrease of the resistivity allows indeed to clearly identify the crystallization onset and completion, as well as the crystallization of the excess Ge which is expelled during the process [38, 65]. As the crystallization temperature strongly increases with C content [65], all GTC films were annealed up to 500°C, temperature at which the crystallization process was found to be complete for all C contents. Pure GeTe was prepared following the same procedure, carrying the annealing up to 450°C, for letting the grain grow (GeTe), and in one case stopping it just after crystallization completion, at $\sim$ 310 °C, and quenching the sample, for stopping the grain growth and obtaining a sample with nanometric grains (nGeTe).

Crystalline structure was investigated by X ray diffraction at the diffraction center Henry Loncharbon (Lyon, France), using a Bruker D8 diffractometer in Bragg-Brentano Geometry with $\lambda = 1.54$ Å and a θ-2θ geometry. LaB_6 and Al_2O_3 powder were used to calibrate the diffractometer resolution. More details are in the Supplementary Material. The Raman signal from amorphous carbon in GTC9 was collected using a LabRAM HR Evolution Raman Spectrometer, from Horiba Scientic, at the Centre Commun de Microspectrometrie Optique (CECOMO) in Lyon, with a laser wavelength of 532 nm, and in a backscattering configuration.

The Hall resistivity, giving access to the charge carrier density, was measured at CEA-LETI SPINTEC varying the magnetic field between -1.5 and +1.5 T, perpendicularly to the surface of the sample. An applied current of 100μA was imposed between two terminals and the voltage measured between the other two, in a Van Der Paw configuration., as a function of the magnetic field.

B. Experimental techniques

Thermal conductivity was measured using the 3ω technique for temperatures from 100 to 300 K on films deposited directly on silicon. A 60 nm thick $Al2O_3$ insulating layer was deposited on the capping SiN layer (20 nm), to perfectly electrically isolate the thermometers. A 5 nm thick adhesion Ti layer was deposited prior to the deposition of the Pt thermometer (95 nm thick). Four different thicknesses from 100 to 1000 nm, were measured for each sample, for disentangling the interface thermal resistance at the sample-substrate/sample-thermometer or sample-transducer interface from the intrinsic signal from the sample [66]. The analysis of the x ray diffraction pattern confirmed that the microstructure was thickness independent. Consistency of thermal measurements results indicate that there is no thickness-dependence of the thermal conductivity at all investigated temperatures between 100 nm and 1 μm, confirming previous results on pure GeTe thin films [39, 67]. For the nGeTe sample, the lower annealing temperature leaves some residual stress in the thin film, which caused its delamination during the technological steps for preparing the 3ω measurements. For this reason, we measured it using the thermoreflectance technique (TR). Measurements were performed on nGeTe deposited directly on silicon. The SiN capping layer was removed and replaced by a 5 nm amorphous carbon layer and 100 nm Au film. 4 different thicknesses were measured to extract the intrinsic nGeTe thermal conductivity [68]. The GeTe material annealed at 450 °C was also measured with the TR to confirm the consistency of results between the two techniques. A value of 3.8(6) $W/(m{\cdot}K)^{-1}$ was obtained, against 4.0(4) $W/(m{\cdot}K)^{-1}$ with the 3ω technique.

Phonon dynamics at room temperature was investigated using Inelastic X ray Scattering (IXS) at the ID28 beamline of ESRF. 1 μm thick films deposited on silicon were mounted vertically and aligned in order to work close to the critical angle and reduce as much as possible the contribution form the substrate. The incoming X-ray wavelength was 0.697 Å and the energy resolution 2.8 meV. The strong small angle scattering hindered the visibility of phonons with energy smaller than 7 meV. The vibrational density of states was measured using the Inelastic X-ray Scattering technique with Nuclear resonance Analysis (IXS-NRA) at the ID18 beamline of ESRF [55]. The same films as measured by IXS were used, mounted horizontally, in a grazing incidence geometry to reduce the substrate contribution. Details on the data treatment and analysis are reported in the Supplementary Material.

Electric resistivity was measured by means of the Van der Paw technique in a He-compressor between 20 and 300 K. Squared 1 cm size thin films were deposited on SOI, and gold contacts were deposited by lithography at the four corners after local removal of the SiN capping layer. The contacts with the measurement setup were thus made by wire-bonding on gold.

C. Theoretical methods

The ab-initio calculation were performed using the VASP package [69], together with PAW potentials [70, 71] and the Perdew-Burke-Ernzerhof (PBE) exchange correlation functional [72]. The planewaves energy cutoff was 227eV. The initial structure of GeTe was fully relaxed until the forces on individual atoms were less than 10-4eV and residual stress tensor values were smaller than 0.01 kBar. To include temperature effects onto the vibrational properties, we performed molecular dynamics simulation for 15ps on a 6x6x6 supercell of 432 atoms for GeTe with Gamma point sampling of the Brillouin zone using a 3fs time step and a Nosé-Hoover thermostat. The TDEP package [73] was used to compute the phonon properties at finite temperature. The TDEP fit of the second and third order forces was performed using 500 equally spaced configurations along the MD trajectory. The rhombohedral unit cell of GeTe was used for calculations. The phonon branches reported in Fig. 3 have been calculated along the high symmetry directions $\Gamma - L$, $\Gamma - X$ and $\Gamma - T$, with L=[0 0.5 0], T=[0.5 0.5 0.5] and X=[0 0.5 0.5] as expressed in the relaxed reciprocal cell units. The absolute value of the directional wavevector has been calculated for plotting the dispersions together with the experimental data.

ACKNOWLEDGMENTS

The authors aknowledge fruitful discussion with A. Tanguy and K. Termentzidis, experimental help by A. Bosak, A. Chumakov and D. Bessas at ESRF. Funding: This work was supported by the ANR (project MAPS-ANR-20-CE05-0046 2019) and from the AURA region (Pack Ambition Recherche, project NanoCharme 2018)

DATA AVAILABILITY

Data are available upon request to the corresponding author.

AUTHOR CONTRIBUTIONS

V.M.G. and P.N. conceived and directed the project. V.M.G. conceived the phonon dynamics investigation, performed the experiments, supervised the experimental data analysis and interpretation. R. Cravero performed the thermal conductivity measurements and analysis, A. Tlili performed the inelastic x ray scattering experiments and analysis. J. Paterson and M. Tomelleri synthesized and characterized the samplesin LETI clean rooms under the supervision of P.N.. Hall measurements were performed at CEA-LETI in the framework of P. Marcello master thesis by P. Noel who is sincerely acknowledged

here. O. Bourgeois supervised the thermal measurements and participated to the discussion and interpretation. F. Hippert supervised the structural characterization and participated to discussions and interpretation. J.-Y. Raty performed the theoretical calculations and participated to discussions and interpretation. V.M.G. wrote the manuscript, the co-authors participated to the revisions.

COMPETING INTERESTS

The authors declare no competing interests.

[1] G. A. Slack, Crc handbook of thermoelectrics (CRC Press; 1st edition (September 30, 1995), 1995) Chap. 34, p. 407.

[2] K. Termentzidis, V. M. Giordano, M. Katsikini, E. Paloura, G. Pernot, D. Lacroix, T. Karakostas, and J. Kioseoglou, Enhanced thermal conductivity in percolating nanocomposites: a molecular dynamics investigation, Nanoscale **10**, 21732 (2018).

[3] Y. Zhang, M. Park, and S.-J. Park, Implication of thermally conductive nanodiamond-interspersed graphite nanoplatelet hybrids in thermoset composites with superior thermal management capability, Scientific Reports **9**, 2893 (2019).

[4] X. Yang, Y. Guo, X. Luo, N. Zheng, T. Ma, J. Tan, C. Li, Q. Zhang, and J. Gu, Self-healing, recoverable epoxy elastomers and their composites with desirable thermal conductivities by incorporating bn fillers via in-situ polymerization, Composites Science and Technology **164**, 59 (2018).

[5] X. Yang, L. Tang, Y. Guo, C. Liang, Q. Zhang, K. Kou, and J. Gu, Improvement of thermal conductivities for pps dielectric nanocomposites via incorporating nh2-poss functionalized nbn fillers, Composites Part A: Applied Science and Manufacturing **101**, 237 (2017).

[6] F. B. Juangsa, Y. Muroya, M. Ryu, J. Morikawa, and T. Nozaki, Comparative study of thermal conductivity in crystalline and amorphous nanocomposite, Applied Phys. Lett. **110**, 253105 (2017).

[7] F. B. Juangsa, Y. Muroya, M. Ryu, J. Morikawa, and T. Nozaki, Thermal conductivity of silicon nanocrystals and polystyrene nanocomposite thin films, Journal Phys. D: Appl. Phys. **49** (2016).

[8] J. Moon and A. J. Minnich, Sub-amorphous thermal conductivity in amorphous heterogeneous nanocomposites, RSC Advances **6**, 105154 (2016).

[9] O. Bourgeois, D. Tainoff, A. Tavakoli, Y. Liu, C.Blanc, M. Boukhari, A. Barski, and E. Hadji, Reduction of phonon mean free path: from low-temperature physics to room temperature applications in thermoelectricity, C. R. Physique **17**, 1154 (2016).

[10] M. Verdier, K. Termentzidis, and D. Lacroix, Crystalline-amorphous silicon nano-composites: nano-pores and nano-inclusions impact on the thermal conductivity, Journal of Applied Physics **119**, 175104 (2016).

[11] M. Jeng, R. Yang, D. Song, and G. Chen, Modeling the thermal conductivity and phonon transport in nanoparticle composites using monte carlo simulation, Journal of Heat Transfer **130**, 042410 (2008).

[12] S. V. Faleev and F. Léonard, Theory of enhancement of thermoelectric properties of materials with nanoinclusions, Phys. Rev. B **77**, 214304 (2008).

[13] W. Xu, Y. Liu, B. Chen, D.-B. Liu, Y.-H. Lin, and A. Marcelli, Nano-inclusions: a novel approach to tune the thermal conductivity of in_2o_3, Physical Chemistry Chemical Physics **15**, 17595 (2013).

[14] G. P. Srivastava and I. O. Thomas, Tunable thermal transport characteristics of nanocomposites, Nanomaterials **10**, 673 (2020).

[15] W. Xu and G. Zhang, Remarkable reduction of thermal conductivity in phosphorene phononic crystal, Journal of Physics: Condensed Matter **28**, 175401 (2016).

[16] A. Tlili, V. M. Giordano, Y. M. Beltukov, P. Desmarchelier, S. Merabia, and A. Tanguy, Enhancement and anticipation of the ioffe-regel crossover in amorphous/nanocrystalline composites, unpublished (2019).

[17] H. Luo, A. Gravouil, V. Giordano, and A. Tanguy, Thermal transport in a 2d nanophononic solid: Role of biphasic materials properties on acoustic attenuation and thermal diffusivity, Nanomaterials **9**, 1471 (2019).

[18] H. Luo, Y. Ren, A. Gravouil, V. M. Giordano, Q. Zhou, H. Wang, and A. Tanguy, Role of a fractal shape of the inclusions on acoustic attenuation in a nanocomposite, APL Materials **9**, 081109 (2021).

[19] L. Yang, N. Yang, and B. Li, NanoLetters **14**, 1734 (2014).

[20] T. Damart, V. M. Giordano, and A. Tanguy, Nanocrystalline inclusions as a low-pass filter for thermal transport ina-si, Physical Review B **92**, 10.1103/physrevb.92.094201 (2015).

[21] W. Schirmacher, T. Scopigno, and G. Ruocco, Theory of vibrational anomalies in glasses, Journal of Non-Crystalline Solids **407**, 133 (2015).

[22] W. Schirmacher, G. Ruocco, and T. Scopigno, Acoustic attenuation in glasses and its relation with the boson peak, Physical Review Letters **98**, 10.1103/physrevlett.98.025501 (2007).

[23] Y. Beltukov, D. Parshin, V. Giordano, and A. Tanguy, Propagative and diffusive regimes of acoustic damping in bulk amorphous material, Physical Review E **98**, 023005 (2018).

[24] H. F. Hamann, M. O'Boyle, Y. C. Martin, M. Rooks, and H. K. Wickramasinghe, Ultra-high-density phase-change storage and memory, Nature Materials **5**, 383 (2006).

[25] P. Noé, C. Vallée, F. Hippert, F. Fillot, and J.-Y. Raty, Phase-change materials for non-volatile memory devices: from technological challenges to materials science issues, Semiconductor Science and Technology **33**, 013002 (2017).

[26] A. Redaelli, ed., *Phase Change Memory: Device Physics, Reliability and Applications* (Springer International Publishing, 2018).

[27] A. Redaelli, ed., *Phase Change Memory* (Springer International Publishing, 2018).

[28] J. Wei, K. Zhang, T. Wei, Y. Wang, Y. Wu, and M. Xiao, High-speed maskless nanolithography with visible light based on photothermal localization, Scientific Reports **7**, 10.1038/srep43892 (2017).

[29] Q. Wang, E. T. F. Rogers, B. Gholipour, C.-M. Wang, G. Yuan, J. Teng, and N. I. Zheludev, Optically reconfigurable metasurfaces and photonic devices based on phase change materials, Nature Photonics **10**, 60 (2015).

[30] J. Li, X. Zhang, X. Wang, Z. Bu, L. Zheng, B. Zhou, F. Xiong, Y. Chen, and Y. Pei, High-performance GeTe thermoelectrics in both rhombohedral and cubic phases, Journal of the American Chemical Society **140**, 16190 (2018).

[31] M. Hong, J. Zou, and Z.-G. Chen, Thermoelectric gete with diverse degrees of freedom having secured superhigh performance, Advanced Materials **31**, 1807071 (2019).

[32] M. Hong, M. Li, Y. Wang, X.-L. Shi, and Z.-G. Chen, Advances in versatile GeTe thermoelectrics from materials to devices, Advanced Materials **35**, 2208272 (2022).

[33] Y. Yu, M. Cagnoni, O. Cojocaru-Mirédin, and M. Wuttig, Chalcogenide thermoelectrics empowered by an unconventional bonding mechanism, Adv. Funct. Mater **30**, 1904862 (2020).

[34] Q. Hubert, C. Jahan, V. Sousa, L. Perniola, A. kusiak, J.-L. battaglia, P. Noé, M. bernard, C. Sabbione, M. Tessaire, F. Pierre, P. Zuliani, R. annunziata, G. Pananakakis, and B. de Salvo, A new insight on ireset reduction of carbon-doped gst based pcm., in *Conf. on Solid State Devices and Materials (SSDM)* (2013) p. 550).

[35] T.-Y. Lee, K. H. P. Kim, D.-S. Suh, C. Kim, Y.-S. Kang, D. G. Cahill, D. Lee, M.-H. Lee, M.-H. Kwon, K.-B. Kim, and Y. Khang, Low thermal conductivity in ge2sb2te5–siox for phase change memory devices, Appl. Phys. Letters **94**, 243103 (2009).

[36] G. B. Beneventi, L. Perniola, V. Sousa, E. Gourvest, S. Maitrejean, J. Bastien, A. Bastard, B. Hyot, A. Fargeix, C. Jahan, J. Nodin, A. Persico, A. Fantini, D. Blachier, A. Toffoli, S. Loubriat, A. Roule, S. Lhostis, H. Feldis, G. Reimbold, T. Billon, B. D. Salvo, L. Larcher, P. Pavan, D. Bensahel, P. Mazoyer, R. Annunziata, P. Zuliani, and F. Boulanger, Carbon-doped GeTe: A promising material for phase-change memories, Solid-State Electronics **65-66**, 197 (2011).

[37] D. Térébénec, N. Bernier, N. Castellani, M. Bernard, J. B. Jager, M. Tomelleri, J. Paterson, M.-C. Cyrille, N.-P. Tran, V. M. Giordano, F. Hippert, and P. Noé, Innovative nanocomposites for low power phase-change memory GeTe/c multilayers, physica status solidi (RRL) – Rapid Research Letters **16**, 10.1002/pssr.202200054 (2022).

[38] R. Chahine, M. Tomelleri, J. Paterson, M. Bernard, N. Bernier, F. Pierre, D. Rouchon, A. Jannaud, C. Mocuta, V. M. Giordano, F. Hippert, and P. Noé, Nanocomposites of chalcogenide phase-change materials: from c doping of thin films to advanced multilayers, Journal of Materials Chemistry C **11**, 269 (2023).

[39] D. Campi, L. Paulatto, G. Fugallo, F. Mauri, , and M. Bernasconi, First-principles calculation of lattice thermal conductivity in crystalline phase change materials GeTe, Sb_2Te_3, and $Ge_2Sb_2Te_5$, Phys. Rev. B **95**, 024311 (2017).

[40] K. Ghosh, A. Kusiak, P. Noé, M.-C. Cyrille, and J.-L. Battaglia, Thermal conductivity of amorphous and crystalline GeTe thin film at high temperature: Experimental and theoretical study, Physical Review B **101**, 10.1103/physrevb.101.214305 (2020).

[41] A. H. Edwards, A. C. Pineda, P. A. Schultz, M. G. Martin, A. P. Thompson, and H. P. Hjalmarson, Theory of persistent, p-type, metallic conduction in c-GeTe, Journal of Physics: Condensed Matter **17**, L329 (2005).

[42] A. J. Bullen, K. E. O'Hara, D. G. Cahill, O. Monteiro, and A. von Keudell, Thermal conductivity of amorphous carbon thin films, Journal of Applied Physics **88**, 6317 (2000).

[43] J. Li, S. J. Kim, S. Han, and H. Chae, Characterization of sp2/sp3 hybridization ratios of hydrogenated amorphous carbon films deposited in c2h2 inductively coupled plasmas, Surface and Coatings Technology **422**, 127514 (2021).

[44] A. Giri, C. J. Dionne, and P. E. Hopkins, Atomic coordination dictates vibrational characteristics and thermal conductivity in amorphous carbon, npj Computational Materials **8**, 10.1038/s41524-022-00741-7 (2022).

[45] P. K. Chu and L. Li, Characterization of amorphous and nanocrystalline carbon films, Materials Chemistry and Physics **96**, 253 (2006).

[46] R. Jana, D. Savio, V. L. Deringer, and L. Pastewka, Structural and elastic properties of amorphous carbon from simulated quenching at low rates, Modelling and Simulation in Materials Science and Engineering **27**, 085009 (2019).

[47] P. B. Pereira, I. Sergueev, S. Gorsse, J. Dadda, E. Müller, and R. P. Hermann, Lattice dynamics and structure of GeTe, SnTe and PbTe, physica status solidi (b) **250**, 1300 (2012).

[48] A. Kusiak, J.-L. Battaglia, P. Noé, V. Sousa, and F. Fillot, Thermal conductivity of carbon doped gete thin films in amorphous and crystalline state measured by modulated photo thermal radiometry, Journal of Physics: Conference Series **745**, 032104 (2016).

[49] A. Snarskii, M. I. Zhenirovskii, and I. V. Bezsudnov, On the wiedemann-franz law in thermoelectric composites, Journal of Thermoelectricity , 57 (2006).

[50] H.-S. Kim, Z. M. Gibbs, Y. Tang, H. Wang, and G. J. Snyder, Characterization of lorenz number with seebeck coefficient measurement, APL Materials **3**, 041506 (2015).

[51] R. Cravero, S. Pailhès, R. Debord, P. Noe, and V. M. Giordano, Thermoelectric properties of gete- amorphous carbon nanocomposites (2).

[52] H. Euchner, S. Pailhès, L. T. K. Nguyen, W. Assmus, F. Ritter, A. Haghighirad, Y. Grin, S. Paschen, and M. de Boissieu, Phononic filter effect of rattling phonons in the thermoelectric clathrate ba8ge40+xni6?x., Phys. Rev. B **86**, 224303 (2012).

[53] P.-F. Lory, S. Pailhès, V. M. Giordano, H. Euchner, H. D. Nguyen, R. Ramlau, H. Borrmann, M. Schmidt, M. Baitinger, M. Ikeda, P. Tomes, M. Mihalkovic, C. Allio, M. R. Johnson, H. Schober, Y. Sidis, F. Bourdarot, L. P. Regnault, J. Ollivier, S. Paschen, Y. Grin, and M. de Boissieu, Long-living heat carriers in a crystalline poor thermal conductor, Nat. Comm. (under review) (2017).

[54] V. M. Giordano and G. Monaco, Fingerprints of order and disorder on the high-frequency dynamics of liquids, PNAS **107**, 21985 (2010).

[55] A. I. Chumakov, A. Q. R. Baron, R. Rüffer, H. Grünsteudel, H. F. Grünsteudel, and A. Meyer, Nu-

clear resonance energy analysis of inelastic x-ray scattering, Phys. Rev. Lett. **76**, 4258 (1996).

[56] T. Chatterji, S. Rols, and U. D. Wdowik, Dynamics of the phase-change material GeTe across the structural phase transition, Frontiers of Physics **14**, 10.1007/s11467-018-0864-1 (2018).

[57] W. A. Kamitakahara and B. N. Brockhouse, Vibrations of a mixed crystal: Neutron scattering from $ni_{55}pd_{45}$, Phys. Rev. B **10**, 1200 (1974).

[58] W. A. Kamitakahara and D. W. Taylor, Comparison of single-site approximations for the lattice dynamics of mass-disordered alloys, Phys. Rev. B **10**, 1190 (1974).

[59] R. Gurunathan, R. Hanus, M. Dylla, A. Katre, and G. J. Snyder, Analytical models of phonon–point-defect scattering, Physical Review Applied **13**, 10.1103/physrevapplied.13.034011 (2020).

[60] Z. Wang, J. E. Alaniz, W. Jang, J. E. Garay, and C. Dames, Thermal conductivity of nanocrystalline silicon: Importance of grain size and frequency-dependent mean free paths, Nano Letters **11**, 2206 (2011).

[61] A. France-Lanord, S. Merabia, T. Albaret, D. Lacroix, and K. Termentzidis, Thermal properties of amorphous/crystalline silicon superlattices, Journal of Physics: Condensed Matter **26**, 355801 (2014).

[62] H. Gu, K. Chen, H. Wang, Z. Li, J. Wang, and X. Wei, Thermal conduction in amorphous/crystalline silicon superlattices: a molecular dynamics study of the size, temperature, and strain effect, Materials Research Express **6**, 115041 (2019).

[63] A. Minnich and G. Chen, Appl. Phys. Lett. **91**, 073105 (2007).

[64] E. Pop, Energy dissipation and transport in nanoscale devices, Nano Research **3**, 147 (2010).

[65] G. B. Beneventi, L. Perniola, V. Sousa, E. Gourvest, S. Maitrejean, J. C. Bastien, A. Bastard, B. Hyot, A. Fargeix, C. Jahan, J. F. Nodin, A. Persico, A. Fantini, D. Blachier, A. Toffoli, S. Loubriat, A. Roule, S. Lhostis, H. Feldis, G. Reimbold, T. Billon, B. D. Salvo, L. Larcher, P. Pavan, D. Bensahel, P. Mazoyer, R. Annunziata, P. Zuliani, and F. Boulanger, Carbon-doped gete: A promising material for phase-change memories, Solid-State Electronics **65-66**, 197 (2011).

[66] J. Paterson, D. Singhal, D. Tainoff, J. Richard, and O. Bourgeois, Thermal conductivity and thermal boundary resistance of amorphous al2o3 thin films on germanium and sapphire, Journal of Applied Physics **127**, 10.1063/5.0004576 (2020).

[67] R. J. Warzoha, B. F. Donovan, N. T. Vu, J. G. Champlain, S. Mack, and L. B. Ruppalt, Nanoscale thermal transport in amorphous and crystalline gete thin-films, Appl. Phys. Lett. **115**, 023104 (2019).

[68] M. Hadi, S. Pailhès, R. Debord, A. Benamrouche, E. Drouard, T. Gehin, C. Botella, J.-L. Leclercq, P. Noe, F. Fillot, and V. Giordano, Transient thermal conductivity in PECVD SiNx at high temperature: The thermal signature of an on-going irreversible modification, Materialia **26**, 101574 (2022).

[69] G. Kresse and J. Hafner, Ab initio molecular-dynamics simulation of the liquid-metal amorphous-semiconductor transition in germanium, Physical Review B **49**, 14251 (1994).

[70] P. E. Blöchl, Projector augmented-wave method, Physical Review B **50**, 17953 (1994).

[71] G. Kresse and D. Joubert, From ultrasoft pseudopotentials to the projector augmented-wave method, Physical Review B **59**, 1758 (1999).

[72] J. P. Perdew, K. Burke, and M. Ernzerhof, Generalized gradient approximation made simple [phys. rev. lett. 77, 3865 (1996)], Physical Review Letters **78**, 1396 (1997).

[73] O. Hellman, P. Steneteg, I. A. Abrikosov, and S. I. Simak, Temperature dependent effective potential method for accurate free energy calculations of solids, Physical Review B **87**, 10.1103/physrevb.87.104111 (2013).